SIMULATION-BASED ANALYSIS AND PREDICTION OF THRUST VECTOR SERVOELASTIC COUPLING

Jeb S. Orr[*], John H. Wall[†], and Timothy M. Barrows[‡]

A method of analysis and prediction of servoelastic coupling in launch vehicles is presented, surveying the discovery and subsequent resolution of a predicted servoelastic resonance phenomenon affecting the NASA Space Launch System launch vehicle at specific flight conditions. A physics-based linearized multibody mechanization of the governing equations is combined with first principles analysis to demonstrate that antisymmetric bending of the solid rocket motors leads to a reduction of equivalent viscous modal damping through coupling with the thrust vector control actuators. The sensitivity to parameters and the effects of the resonance phenomenon on flight control performance and stability are confirmed through extensive simulation verification in the time and frequency domain. A novel enhancement in model fidelity that accounts for Coriolis effects of fluid flow on bending within the solid rocket motor case and nozzle is shown to add sufficient damping to reduce the risk of adverse control-structure interaction.

1 INTRODUCTION

The dynamic coupling of thrust-vectored rocket engines with a launch vehicle structure is a topic of great interest to vehicle designers, particularly to ensure stable flight control and the design of robust structures that can survive stressful launch environments. During the booster flight control certification process, successful stabilization of primary dynamic response mechanisms receives significant scrutiny. These dynamics include a statically unstable rigid body airframe, primary lateral bending modes of the vehicle structure, and liquid propellant sloshing modes. Secondary effects include stabilization of the thrust vector control (TVC) load resonances, assessment of sample rate aliasing and local sensor mount compliance effects, and interactions among various software algorithms.

Usually of secondary importance are the coupling effects of multiple engines interacting with the structure. These effects often do not manifest unless the moving mass of vectored engines is a substantial fraction of the vehicle mass, the TVC actuator bandwidth is relatively high, or both. There exists a phenomenon known as thrust vector servoelasticity (TVSE), named in analogy to its equivalent in aircraft dynamics, aeroservoelasticity (ASE). In this coupling mechanism, a TVC system resonance is close to a structural bending mode, and the moving mass of the vectored rocket nozzle exerts both thrust and inertial coupling forces and torques on the vehicle structure. The elastic response of the vehicle subsequently imparts coupling torques about the engine gimbal. Since the

[*]Space Launch System Flight Dynamics and Control Technical Specialist, NASA Marshall Space Flight Center / EV41 Control Systems Design and Analysis Branch (Mclaurin Aerospace - Jacobs ESSCA), Huntsville, AL

[†]Space Launch System Controls Working Group Deputy Lead, NASA Marshall Space Flight Center / EV41 Control Systems Design and Analysis Branch (Dynamic Concepts, Inc. - Jacobs ESSCA), Huntsville, AL

[‡]Principal Member of the Technical Staff, Draper (Retired), Cambridge, MA

lateral thrust force is proportional to the engine angle, the lag between the structural motion and the thrust vector can, in the correct circumstances, extract energy from the thrust and reduce the structural damping, or destabilize, the bending dynamics.

For simplified assessments, this relationship can be demonstrated analytically for a simplified system using the Routh criterion. In terms of the sensitivity to external load torques, most TVC systems approximate second-order systems asymptotically in frequency. The engine's compliance to a static external load torque is usually a constant, and at some frequency above the actuator dynamics, the system behaves as an inertial load with an asymptotic frequency response of -40 $\mathrm{dB/dec}$. There exists some frequency where the TVC system response to external load torques is out of phase with the input by $\pi/2$. This frequency is the TVC resonant frequency.

These asymptotic relationships hold regardless of the complexity of the TVC system model, so potential sensitivities can be assessed using a second-order TVC system model with the natural frequency adjusted to match the TVC resonant frequency of a more complex model.

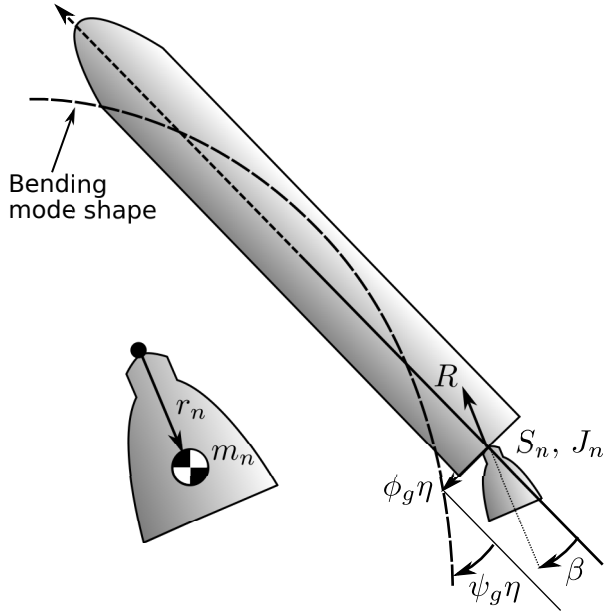

Figure 1. Bending Mode with Thrust Vectoring Nozzle

Consider the dynamics of a hypothetical second-order TVC actuator and a single bending mode (Figure 1). The linearized equations are given by

$$J_n\ddot{\beta} + C_a\dot{\beta} + K_a\beta = -\left(J_n\psi_g + S_n\phi_g\right)\ddot{\eta} \tag{1}$$

$$\ddot{\eta} + 2\zeta_b\omega_b\dot{\eta} + \omega_b^2\eta = -\left(J_n\psi_g + S_n\phi_g\right)\ddot{\eta} - R\phi_g\beta \tag{2}$$

where $S_n = m_n r_n$, J_n are the first and second moments of the inertia about the nozzle pivot, β is the thrust structure relative gimbal angle, and $K_a = J_n\omega_n^2$, $C_a = 2\zeta\sqrt{J_n K_a}$ are the closed-loop engine dynamic parameters.[1] The elastic mode is described by its generalized displacement η, its natural frequency ω_b, and a viscous damping ratio ζ_b. The gimbaled thrust force R is assumed constant, and the elastic parameters of interest are the modal displacement and rotation at the gimbal point, ϕ_g and ψ_g, respectively.

Letting the inertial coupling coefficient $\Upsilon = (J_n\psi_g + S_n\phi_g)$, the coupled equations are described in Laplace notation as

$$\begin{bmatrix} J_n s^2 + C_a s + K_a & \Upsilon s^2 \\ \Upsilon s^2 + \phi_g R & s^2 + 2\zeta_b\omega_b s + \omega_b^2 \end{bmatrix} \begin{bmatrix} \beta \\ \eta \end{bmatrix} = \begin{bmatrix} 0 \\ 0 \end{bmatrix} \tag{3}$$

with the associated characteristic polynomial $\sum a_k s^k = 0$. The roots of this simplified equation can be used to predict the potential magnitude of servoelastic coupling. For example, it can be shown that the critical thrust

$$R < \frac{J_n\left(\omega_n^2 + (2\zeta_n\omega_n)\,(2\zeta_b\omega_b) + \omega_b^2\right)}{\Upsilon\phi_g} \tag{4}$$

is a necessary condition for stability of the coupled system.

It must be emphasized that a thrust vector servoelastic resonance involves only thrust, the vehicle dynamics, engine dynamics, and TVC hardware. Since TVSE involves only inner loop (servo) feedback, there are no software or avionics components involved. The TVSE phenomenon can occur even if the autopilot is not providing feedback, although depending on the observability and frequency of the mode in question, flight control feedback can either worsen or improve the situation.

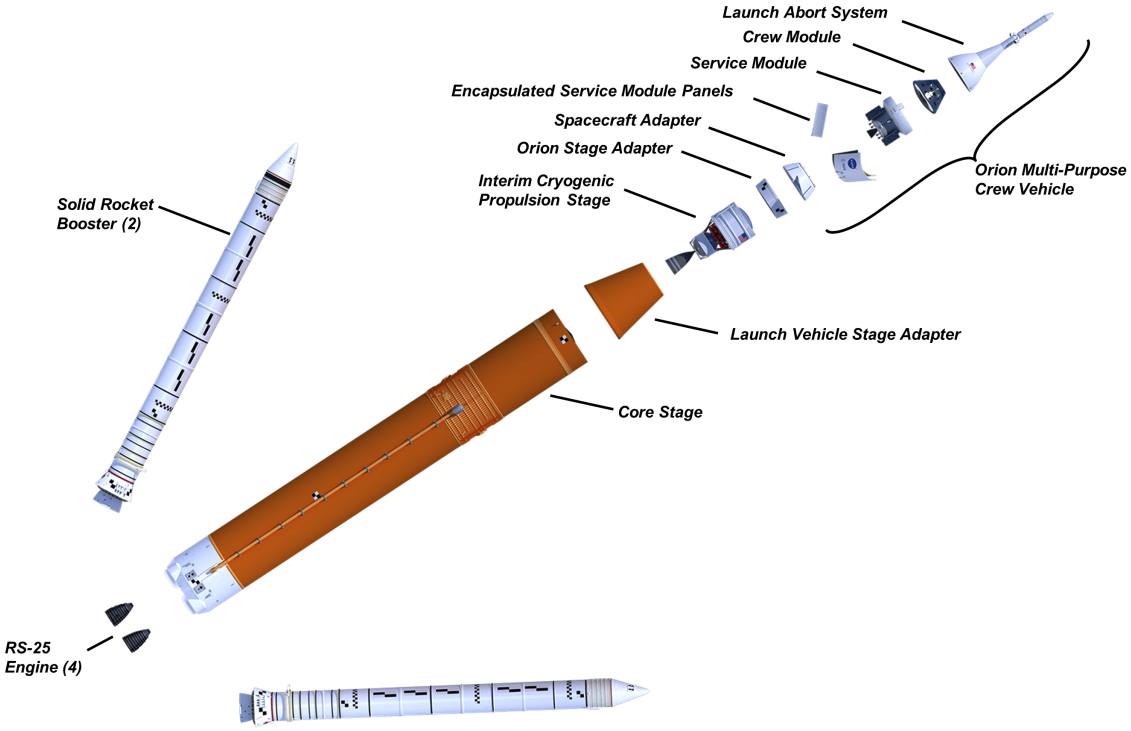

Figure 2. Space Launch System Block 1 Configuration (NASA)

2 SPACE LAUNCH SYSTEM

The Space Launch System (SLS) is NASA's next-generation exploration-class launch vehicle for space access, including such objectives as human transit to Mars, rendezvous with near-earth asteroids, and the launch of unmanned probes to distant solar system targets such as Europa. Its design

provides for a level of performance and reliability that is unmatched in any existing or planned launch system, including an ability to loft approximately 57,000 lbm to trans-lunar injection (TLI) in its initial Block 1 configuration (Figure 2). Its evolved configurations, Block 1B and Block 2, utilize the Exploration Upper Stage (EUS) to increase performance. The Block 1B with EUS has a cargo payload performance capability of approximately 88,000 lbm to TLI. The Block 2, more than 375 feet long and using upgraded solid rocket motors (SRMs), is able to loft 290,000 lbm to low Earth orbit (LEO) or 99,000 lbm to a heliocentric orbit.

The SLS leverages hardware, processes, and design concepts derived from the Saturn and Space Shuttle programs, including an 27.5 ft diameter core stage containing more than 700,000 gallons of cryogenic propellants.[2] The core stage is powered by four RS-25E liquid engines derived from the Space Shuttle Main Engine (SSME), each producing about 475,000 lbf of thrust.[3] Additional thrust is provided by two 5-segment Reusable Solid Rocket Motor-V boosters (RSRMVs). Each booster provides a peak sea level thrust of about 3.3 million lbf and provides primary ascent propulsion during the 126-second boost phase. Three-axis control and stabilization during powered flight is provided by coordinated thrust vectoring of the solid rocket nozzles as well as all four RS-25E core stage engines, using 12 Space Shuttle heritage quad-redundant hydraulic actuators.

3 ANALYSIS

Analysis of the Space Launch System transient flight dynamics and stability is performed in an analytically linearized multibody dynamics model. The FRACTAL (Frequency Response Analysis and Comparison Tool Assuming Linearity) model was developed at NASA MSFC using a rigorous, matrix-vector Lagrangian derivation of the equations of motion that reduces to the classical planar rocket equations of motion as a special case.[4]

Classical methods develop the system equations via superposition using an *integrated body* approach.[5] The orthogonal vibration modes are elicited from a finite element model containing all of the vehicle mass, including the gimbaled engines. After partitioning, the rigid body degrees of freedom, as well as some of the other dynamic modes, are replaced with a higher-fidelity set of equations to model effects not represented in the FEM, e.g., aerodynamics, propellant slosh, sensors, and servoactuators.

The inertial engine coupling dynamics are of key concern in the formulation of a physics-based model. The presence of a servoactuator position control loop substantially changes the character of the engine dynamic modes, and this effect cannot be duplicated with a simple spring approximation of the actuator. If the engine dynamic modes are strongly coupled with the global vehicle bending, it is advantageous to use a more advanced approach to developing the equations of motion.

In a *reduced-body* method, finite element modes, generated from a model with engines removed, are coupled to a dynamic model of the engines, propellant, and airframe. The compliance within the actuator load path, including the backup structure, can be more accurately modeled. Since certain orthogonality conditions cannot be assumed, additional terms must be included in the equations of motion to recover the correct dynamics. The engine states are integrated simultaneously with the vehicle dynamics; that is, the engine equations are part of the system mass matrix. This allows the direct and simultaneous solution of the equations describing the engine and global bending dynamics, but the local engine and backup structure compliance remains within the servoactuator model.

Since the global bending modes need not model the backup compliance, there are no special

requirements placed on the mode shapes such that they include high-fidelity information at the actuator attach points. The nozzle is instead coupled to the vehicle using a virtual torque-torque interface. Given computational constraints, the selection of a subset of modes for flight control analysis can be focused on those most relevant for global feedback stability rather than the dynamics of the servoactuator loop. Conversely, the servoactuator model can be coupled to the engine using only angular position and torque feedback, and can internally use an arbitrarily complex representation of the load compliance and servodynamics.*

A total of three novel developments are used to analyze TVSE, or the dynamic interaction of the booster TVC with the vehicle structure: the fully-coupled reduced-body formulation for the engine dynamics, the incorporation of propellant flow turning (jet damping) effects, and the use of thrust structure mode shapes and geometry to construct virtual spatial derivatives of the eigenvectors.

3.1 Reduced-Body Equations of Motion

The linearized motion equations of coupled bending and engine dynamics presented here are a subset of the multi-DoF formulation used in the FRACTAL toolchain. The motion equations are expressed in a trajectory-relative accelerating frame, which depends on the mean vehicle acceleration $\mathbf{g}_0$. While the fully-coupled model with slosh and aerodynamics is used to evaluate TVSE in production analyses, the following two equations are sufficient to capture the phenomenon in three dimensions. The engine and bending equations are given by

$$\begin{aligned}\mathbf{J}^{\mathcal{G}}_{ei}\dot{\boldsymbol{\omega}}_{\mathcal{G}ei} + \mathbf{D}_{ei}\boldsymbol{\omega}_{\mathcal{G}ei} + \left(\mathbf{K}_{ei} + m_{ei}\mathbf{g}_0^{\times}\mathbf{r}^{\times}_{\mathcal{G}ei}\right)\boldsymbol{\Theta}_{\mathcal{G}ei} = \\ \underbrace{\boldsymbol{\tau}_{ei}}_{\text{actuator}} \underbrace{- m_{ei}\mathbf{r}^{\times}_{\mathcal{G}ei}\dot{\mathbf{v}}^{\mathcal{T}} - \left(\mathbf{J}^{\mathcal{G}}_{ei} - m_{ei}\mathbf{r}^{\times}_{\mathcal{G}ei}\mathbf{r}^{\times}_{\mathcal{G}i}\right)\dot{\boldsymbol{\omega}}}_{\text{DWT}} \underbrace{- \left(m_{ei}\mathbf{r}^{\times}_{\mathcal{G}ei}\boldsymbol{\Phi}_{\mathcal{G}i} + \mathbf{J}^{\mathcal{G}}_{ei}\boldsymbol{\Psi}_{\mathcal{G}i}\right)\ddot{\boldsymbol{\eta}}}_{\text{DWT (flex)}}\end{aligned} \quad (5)$$

$$\begin{aligned}\left(\mathbf{I}_k + \bar{\boldsymbol{\Gamma}}_{ei}m_{ei}\boldsymbol{\Gamma}_{ei} + \bar{\boldsymbol{\Psi}}_{\mathcal{G}i}\left(\mathbf{J}^{\mathcal{G}}_{ei} + m_{ei}\mathbf{r}^{\times}_{\mathcal{G}ei}\mathbf{r}^{\times}_{\mathcal{G}ei}\right)\boldsymbol{\Psi}_{\mathcal{G}i}\right)\ddot{\boldsymbol{\eta}} + 2\zeta\boldsymbol{\Omega}\dot{\boldsymbol{\eta}} + \boldsymbol{\Omega}^2\boldsymbol{\eta} = \\ \underbrace{- \bar{\boldsymbol{\Phi}}_{\mathcal{G}i}R_{ei}\mathbf{u}^{\times}_{ei}\boldsymbol{\Theta}_{\mathcal{G}ei}}_{\text{thrust}} \underbrace{- \left(\bar{\boldsymbol{\Psi}}_{\mathcal{G}i}\mathbf{J}^{\mathcal{G}}_{ei} - \bar{\boldsymbol{\Phi}}_{\mathcal{G}i}m_{ei}\mathbf{r}^{\times}_{\mathcal{G}ei}\right)\dot{\boldsymbol{\omega}}_{\mathcal{G}i}}_{\text{TWD (flex)}} + \mathbf{Q}_p \\ - \bar{\boldsymbol{\Gamma}}_{ei}m_{ei}\dot{\mathbf{v}}^{\mathcal{T}} + \left(m_{ei}\bar{\boldsymbol{\Phi}}_{\mathcal{G}i}\left(\mathbf{r}_{\mathcal{G}i} + \mathbf{r}_{\mathcal{G}ei}\right)^{\times} + \bar{\boldsymbol{\Psi}}_{\mathcal{G}i}\left(\mathbf{r}^{\times}_{\mathcal{G}ei}m_{ei}\mathbf{r}^{\times}_{\mathcal{G}i} - \mathbf{J}^{\mathcal{G}}_{ei}\right)\right)\dot{\boldsymbol{\omega}}\end{aligned} \quad (6)$$

where the angular rate dynamics of the i^{th} of r engines are written with respect to each gimbal, $\boldsymbol{\omega}_{\mathcal{G}ei}$, and is subsequently truncated to two degrees of freedom. The engine without actuator dynamics is described by its inertia tensor $\mathbf{J}^{\mathcal{G}}_{ei}$, a damping matrix $\mathbf{D}_{ei}$, and a stiffness matrix $\mathbf{K}_{ei}$, typically representing flex bearing stiffness. The virtual gimbal shape $\boldsymbol{\Phi}_{\mathcal{G}i}$ and virtual gimbal slope $\boldsymbol{\Psi}_{\mathcal{G}i}$ are computed as a function of the rotation and translation eigenvectors at the gimbal and two actuator backup attach grids. The acceleration $\dot{\mathbf{v}}^T$ is a trajectory-relative perturbation acceleration of the vehicle, $\boldsymbol{\omega}$ is the body angular rate, and $\boldsymbol{\eta} \in \mathbb{R}^k$ is the elastic generalized displacement.

The mean acceleration $\mathbf{g}_0$ of the engine gimbal provides an equivalent gravitational stiffening torque. The angular and lateral acceleration of the vehicle impart inertial coupling torques at the engine attach point known as "dog-wag-tail" or DWT, and an equivalent coupling due to generalized acceleration of the gimbal point that depends on the bending dynamics. Local actuator torques are represented by a generalized force $\boldsymbol{\tau}_{ei}$ that, in general, depends on the engine and actuator states.

*A complementary approach developed by the authors, where the servoactuator is directly coupled with a high-fidelity FEM using thousands of modes, is the method used in the MSFC MASV (Multiple Actuator Stage Vectoring) simulation.

The bending equations (6) include coupling terms (in red) that arise when the engine masses are not included in the finite element model. The term $\mathbf{\Gamma}_{ei} = \mathbf{\Phi}_{\mathcal{G}i} - \mathbf{r}_{ei}^{\times}\mathbf{\Psi}_{Gi}$ is the elastic coupling matrix at the i^{th} engine, which is used to form an augmented mass matrix for the mass-normalized bending dynamics, where $\mathbf{\Omega}^2$ is the (diagonal) generalized stiffness matrix. The basic elastic damping ζ is typically assumed constant across all modes. Typically, $\zeta = 0.005$ for control-structure interaction analysis on large boosters.

In the elastic equation, $\bar{\mathbf{\Phi}}$, $\bar{\mathbf{\Psi}}$ denote the transpose of the mode shape and slope matrices, respectively. The propellant flow (jet damping) generalized forces are incorporated into the term $\mathbf{Q}_p$, which can be expressed as a linear function of $\dot{\boldsymbol{\eta}}$ and $\boldsymbol{\omega}_{\mathcal{G}ei}$. When incorporated into a model containing the rigid-body and sloshing degrees of freedom, these equations can reproduce the TVSE resonance as a function of the system parameters and the flight condition. As suggested earlier, these degrees of freedom are sufficient to model TVSE, although the predictions tend to be conservative; coupling with the rigid body and sloshing dynamics is an energy sink and tends to add damping across all coupled system modes.

3.2 Elastic Jet Damping

The term *jet damping* is traditionally associated with the rigid-body pitch or yaw rate of a rocket or rocket nozzle. It is the torque due to the expulsion of propellant through the nozzle, which almost always has the effect of damping out a given rotation rate. Simplified analyses view it as the result of a force applied at the nozzle exit plane. However, this effect is more accurately seen as arising from the integrated effect of Coriolis forces acting along the interior path of the propellant. The notion of integrating the forces along the entire length is essential for computing the damping of flexible motion.[6]

Consider a differential element of propellant dm in the core of a flexible booster having a case length L. Since the burning propellant is confined to travel parallel to the centerline of the booster, whose structure is elastically deforming with respect to an inertial frame, the propellant undergoes an acceleration. Hypothetical profiles of dynamic quantities along the centerline of the RSRMV are depicted in Figure 3. The axes in this diagram are chosen such that $x = 0$ corresponds to the foremost location of propellant. A representative z component of the mode shape $\Phi_z(x)$ is depicted, and the velocity of the flow $U(x)$ varies throughout the case and nozzle. Along the length of burning propellant from $x = 0$ to $x = L$, the mass flow is assumed to vary linearly from zero to its maximum value $\dot{m}_e$ at the nozzle throat, and is constant through the nozzle section. It should be noted that such a model is valid for the RSRMV based on its actual burning profile at the flight condition in question, although it may not hold for all solid rocket motor designs.

Under reasonable assumptions, including ignoring boundary layer shear forces, it can be shown that the material derivative along the length of the case is given by

$$\frac{D\mathbf{u}}{Dt} = \mathbf{\Phi}\ddot{\boldsymbol{\eta}} - 2U\hat{\mathbf{i}}^{\times}\mathbf{\Psi}\dot{\boldsymbol{\eta}} + U\frac{dU}{dx}\hat{\mathbf{i}} - \hat{\mathbf{i}}^{\times}\left(U^2\frac{d\mathbf{\Psi}}{dx} + U\frac{dU}{dx}\mathbf{\Psi}\right)\boldsymbol{\eta} \tag{7}$$

The stiffening and apparent mass effects are easily shown to be insignificant for a problem of this scale, leaving only terms that are relevant to damping. Letting dm be the fluid mass within a lamina dx as shown in Figure 3, and assuming no dependency on the coordinates normal to the flow,

$$\frac{D\mathbf{u}}{Dt}dm = -2U\hat{\mathbf{i}}^{\times}\mathbf{\Psi}\dot{\boldsymbol{\eta}}\rho A\,dx \tag{8}$$

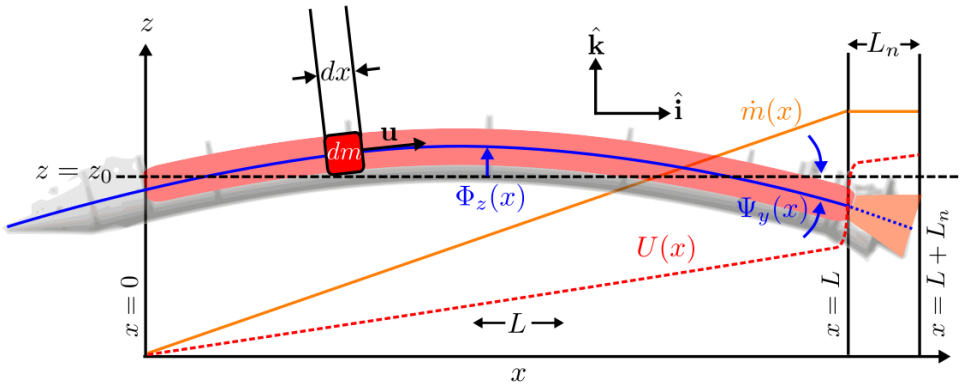

Figure 3. Dynamic Elements Affecting Jet Damping

where ρ is the gas density and A is the cross section area. The local mass flow rate $\dot{m}(x) = U\rho A$, thus

$$d\mathbf{f} = 2\hat{\mathbf{i}}^{\times}\boldsymbol{\Psi}\dot{\boldsymbol{\eta}}\dot{m}\,dx \tag{9}$$

which depends only on the mass flow profile. The generalized force $\mathbf{Q}_p \in \mathbb{R}^k$ due to propellant in the elastic equation is given by

$$d\mathbf{Q}_p(x) = \bar{\boldsymbol{\Phi}}(x)d\mathbf{f}(x) \tag{10}$$

Let $\mathbf{Q}_{ci}$ and $\mathbf{Q}_{ni}$be the generalized force due to jet damping within the i^{th} case and the i^{th} nozzle, respectively, and the total jet damping effect is given by$\mathbf{Q}_p = \sum \mathbf{Q}_{ci} + \sum \mathbf{Q}_{ni}$. Inserting (9) into (10) and integrating, the case component becomes

$$\mathbf{Q}_{ci} = 2\left\{\int_0^L \dot{m}(x)\bar{\boldsymbol{\Phi}}(x)\hat{\mathbf{i}}^{\times}\boldsymbol{\Psi}(x)\,dx\right\}\dot{\boldsymbol{\eta}}.$$

We now apply the aforementioned assumption that the local mass flow rate is zero at the head end of the booster case $x = 0$ and increases linearly with x until it reaches the total mass flow rate $\dot{m}_e$ at $x = L$. That is,

$$\dot{m}(x) = \dot{m}_e\frac{x}{L} \tag{11}$$

Thus

$$\mathbf{Q}_{ci} = \dot{m}_e\left\{\frac{2}{L}\int_0^L x\bar{\boldsymbol{\Phi}}(x)\hat{\mathbf{i}}^{\times}\boldsymbol{\Psi}(x)\,dx\right\}\dot{\boldsymbol{\eta}}. \tag{12}$$

In a linear, time-invariant model the quantity in brackets is a linear matrix coefficient of $\dot{\boldsymbol{\eta}}$. For the nozzle, the computation of the integral is similar, but the mass flow is assumed constant as no propellant burning occurs upon exiting the case. In addition, the nozzle rotates with respect to the thrust structure with an angular rate that depends on the nozzle rigid body states. The generalized force due to elastic motion of the i^{th} nozzle is given by

$$\mathbf{Q}_{ni} = 2\dot{m}_e L_n\bar{\boldsymbol{\Phi}}_{\mathcal{G}i}\hat{\mathbf{i}}^{\times}\left(\boldsymbol{\Psi}_{\mathcal{G}i}\dot{\boldsymbol{\eta}} + \boldsymbol{\omega}_{\mathcal{G}i}\right) \tag{13}$$

where L_n is the nozzle length. The matrix form of this expression can also be incorporated into the damping and actuator coupling matrices in the bending equations.

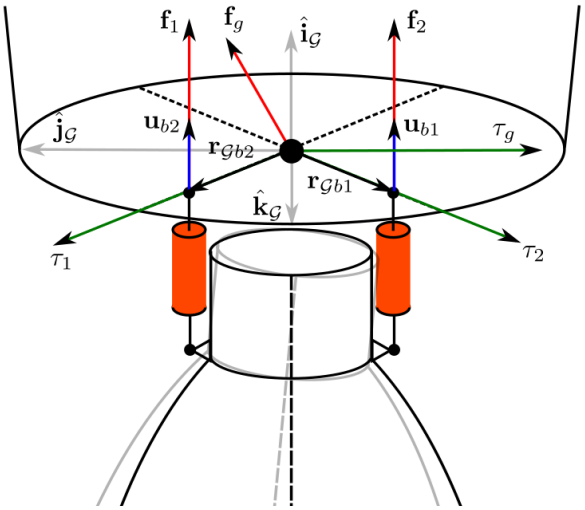

Figure 4. IVG Method Thrust Structure Geometry

Computation of the integral in Equation 12 requires a numerical approximation, since the modal data are given at discrete centerline grids along the booster axial coordinate. A trapezoidal integration approximation is used;

$$\mathbf{Q}_{ci} \approx \dot{m}_e \frac{1}{L} \sum_{j=1}^{N-1} (x_{j+1} - x_j) \left(x_{j+1} \bar{\mathbf{\Phi}}_{c,\,j+1} \hat{\mathbf{i}}^{\times} \mathbf{\Psi}_{c,\,j+1} + x_j \bar{\mathbf{\Phi}}_{c,\,j} \hat{\mathbf{i}}^{\times} \mathbf{\Psi}_{c,\,j} \right) \dot{\boldsymbol{\eta}} \tag{14}$$

over N discrete stations distributed, in general, non-uniformly down the centerline of each booster. Here, the subscript c is used distinguish from the previous gimbal point parameters. The resultant matrix is computed at each analysis time using the instantaneous mass flow $\dot{m}_e$, which varies in time and may also vary from booster to booster.

3.3 Improved Virtual Grid (IVG) Model

As discussed in the preceding sections, inertial coupling between the nozzle body and the elastic vehicle structure is modeled using a torque-torque interface. That is, the nozzle is modeled as a linearized pendulum. In such a model, the "gimbal point" includes the local structure and actuators, which transfer loads between the engine, the backup structure, and the thrust application point.

In classical launch vehicle dynamics models[5] it is typical to use a single finite element node to compute the elastic translation and rotation of the structure to which an engine is attached. In practice, the finite element model contains millions of nodes, and the rotation eigenvector of a single FEM grid point does not adequately represent the equivalent torques involving the engine gimbal and actuator attach points. As such, it is necessary to compute a mapping of forces and torques, or equivalently, inertial accelerations, into generalized accelerations of the structural model that accurately reflects the physical configuration of the structure.

A virtual mode slope is an equivalent rotation eigenvector computed at the gimbal point that represents bulk motion of the thrust structure. It is intended to capture only global rotations, not local differential rotations of the associated gimbal and actuator attach grids. A constrained force-

based virtual grid method, or Improved Virtual Grid (IVG), provides a physics-based approach to deriving the gimbal mode slope.

The geometry of the improved virtual grid method is shown in Figure 4. It is desired to compute a virtual grid $\mathbf{\Psi}_{\mathcal{G}} \in \mathbb{R}^{3\times k}$. It is assumed that forces $\mathbf{f}_i$ at the actuator attach points have magnitudes f_i acting along unit directions $\mathbf{u}_{bi}$, which are collinear with the actuator action line at a given static gimbal rotation (usually zero). The geometric relationship of the actuator backup attach points and the gimbal is given by $\mathbf{r}_{\mathcal{G}bi}$.

The problem is constructed as follows: given an applied torque $\boldsymbol{\tau}_g$, resolve the applied torque into force components along the actuator action lines $\mathbf{u}_{bi}$ and an arbitrarily oriented vector force $\mathbf{f}_g$ at the gimbal. The gimbal torque component due to each actuator is $\boldsymbol{\tau}_i = \mathbf{r}^{\times}_{\mathcal{G}bi} f_i \mathbf{u}_{bi}$. Assuming the thrust structure is rigid,[†] the internal forces must sum to zero; $\mathbf{f}_1 + \mathbf{f}_2 + \mathbf{f}_g = \mathbf{0}$. Let the unknowns be $\mathbf{x} = \begin{bmatrix} f_1 & f_2 & \mathbf{f}_g \end{bmatrix}^T \in \mathbb{R}^5$;in matrix form, this problem can be written as

$$\begin{aligned} \begin{bmatrix} \mathbf{r}^{\times}_{\mathcal{G}b1}\mathbf{u}_{b1} & \mathbf{r}^{\times}_{\mathcal{G}b2}\mathbf{u}_{b2} & \mathbf{0}_3 \end{bmatrix} \mathbf{x} &= \mathbf{A}\mathbf{x} = \boldsymbol{\tau}_{\mathbf{g}} \\ \begin{bmatrix} \mathbf{u}_{b1} & \mathbf{u}_{b2} & \mathbf{I}_3 \end{bmatrix} \mathbf{x} &= \mathbf{C}\mathbf{x} = \mathbf{0} \end{aligned} \tag{15}$$

Fortunately, this is a linearly constrained least squares (LS) problem which has a unique solution.[7] The solution minimizes $\|\mathbf{A}\mathbf{x} - \boldsymbol{\tau}_g\|^2$ subject to $\mathbf{C}\mathbf{x} = \mathbf{0}$. Using the Karush-Kuhn-Tucker (KKT) conditions with Lagrange multipliers λ,

$$\begin{bmatrix} \mathbf{x} \\ \lambda \end{bmatrix} = \begin{bmatrix} 2\bar{\mathbf{A}}\mathbf{A} & \bar{\mathbf{C}} \\ \mathbf{C} & \mathbf{0} \end{bmatrix}^{-1} \begin{bmatrix} 2\bar{\mathbf{A}}\boldsymbol{\tau}_g \\ \mathbf{0} \end{bmatrix}. \tag{16}$$

The KKT matrix in Equation 16 is guaranteed invertible if $\mathbf{r}_{\mathcal{G}bi}$, $\mathbf{u}_{bi}$ are linearly independent. Since the solution $\mathbf{x}$ is linear in $\boldsymbol{\tau}_g$ the Jacobian $\partial x_i/\partial \tau_{gi}$ can be computed; let the KKT matrix

$$\mathbf{L} = \begin{bmatrix} \mathbf{L}_{11} & \mathbf{L}_{12} \\ \mathbf{L}_{21} & \mathbf{L}_{22} \end{bmatrix} = \begin{bmatrix} 2\bar{\mathbf{A}}\mathbf{A} & \bar{\mathbf{C}} \\ \mathbf{C} & \mathbf{0} \end{bmatrix}^{-1} \tag{17}$$

such that the solution $\mathbf{x} = \mathbf{L}_{11} 2\bar{\mathbf{A}}\boldsymbol{\tau}_g = \mathbf{M}\boldsymbol{\tau}_g$ where $\mathbf{M}$ is the desired Jacobian. The matrix $\mathbf{M}$ can thereafter be partitioned as

$$\mathbf{M} = \begin{bmatrix} \mathbf{m}_{f1} \\ \mathbf{m}_{f2} \\ \mathbf{M}_{\mathbf{f}_g} \end{bmatrix} \in \mathbb{R}^{5\times 3} \tag{18}$$

and the two scalar and one vector components of the solution are used to find

$$\mathbf{f}_1 = \mathbf{u}_{b1}\mathbf{m}_{f1}\boldsymbol{\tau}_g \tag{19}$$

$$\mathbf{f}_2 = \mathbf{u}_{b2}\mathbf{m}_{f2}\boldsymbol{\tau}_g \tag{20}$$

$$\mathbf{f}_g = \mathbf{M}_{\mathbf{f}_g}\boldsymbol{\tau}_g. \tag{21}$$

In this form, it is clear that the action line and gimbal reaction forces are an explicit linear function of the applied torque.

Using the shape functions to map these physical forces into generalized coordinates, it follows that $\mathbf{Q}_g = \bar{\mathbf{\Psi}}_{\mathcal{G}}\boldsymbol{\tau}_g$ with the virtual grid

$$\bar{\mathbf{\Psi}}_{\mathcal{G}} = \bar{\mathbf{\Phi}}_0\mathbf{M}_{\mathbf{f}_g} + \bar{\mathbf{\Phi}}_{b1}\mathbf{u}_{b1}\mathbf{m}_{f1} + \bar{\mathbf{\Phi}}_{b2}\mathbf{u}_{b2}\mathbf{m}_{f2}. \tag{22}$$

This procedure is used for each set of engine data in order to compute $\mathbf{\Psi}_{\mathcal{G}i}$ used in FRACTAL.

[†]This assumption is intentional as the backup structure compliance is accounted for in the actuator model.

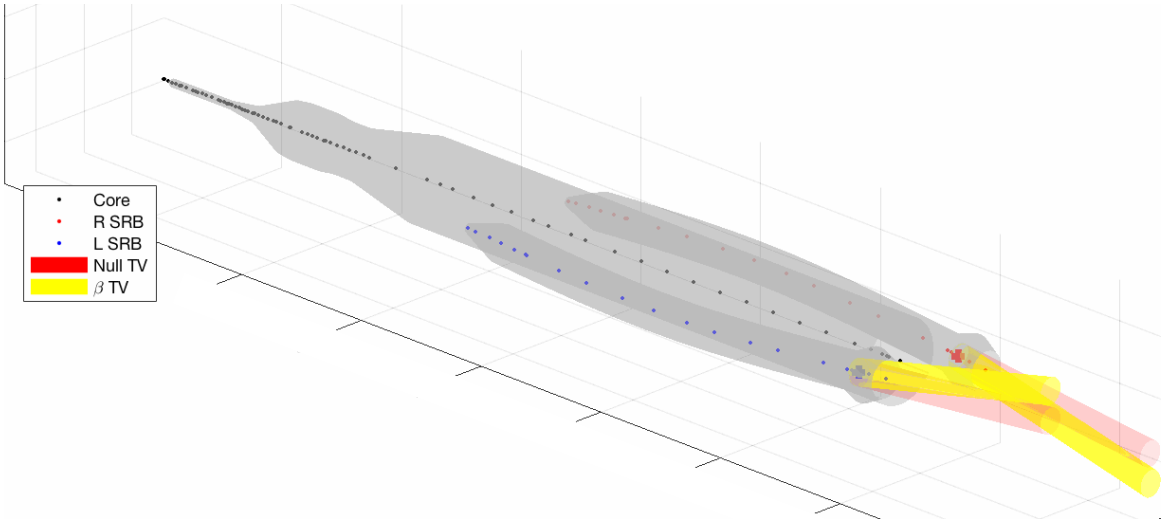

Figure 5. SLS TVSE Antisymmetric Mode (Scale Factors: 20x displacement, 40x TVC angle)

4 SIMULATION

The phenomenon of unstable or marginally-stable servoelastic resonance involving the RSRMV has been known since around 2009, when dog-wag-tail (DWT) models were incorporated during analysis of the Constellation Ares I configuration. In that configuration, the resonance appeared as a gain increase in the vehicle pitch channel at about 80 seconds flight time. It was initially assumed that the apparent resonance was an artifact of a poorly conditioned constraint in the booster structural finite element model.

The investigation was reopened in 2016 when a discrepancy was uncovered in during a multi-center, multi-simulation NASA verification exercise that suggested the presence of a high gain in the roll autopilot channel when DWT was enabled. Since the default simulation configuration did not simulate DWT dynamics for the boosters, the roll mode in question was not present in the baseline. DWT simulation in the baseline for the booster engines confirmed the presence of the roll mode, and a deep-dive analysis was conducted in cooperation with the Space Launch System structural dynamics team. Subsequent analysis using a multifaceted approach to resolving the discrepancy revealed that the issue was physical.

The SLS TVSE mode displacement field and its associated gimbal angles are shown in Figure 5. Adverse coupling of the SLS structure and the booster actuators occurs in late boost flight. The structural mode involved in TVSE is a fundamental antisymmetric bending of the booster case coupled with torsion about the core stage structure. While normally such a coupling phenomenon would involve only hydraulic-structural feedback, the torsion response of the core stage also involves the vehicle autopilot roll gyro. Thus, the autopilot design must also consider the reduced damping of a primary torsional mode resulting from TVSE (Figure 6).

Upon the discovery of the TVSE phenomenon in the SLS vehicle, the program was required to demonstrate, with margin, negligible risk to the flight control system or vehicle loads. The analysis process leveraged the advanced models detailed above, a detailed assessment of the uncoupled structural damping of the subject antisymmetric mode, and a fidelity improvement in the mass properties model for booster nozzles to account for liner ablation. Since the coupling mechanism

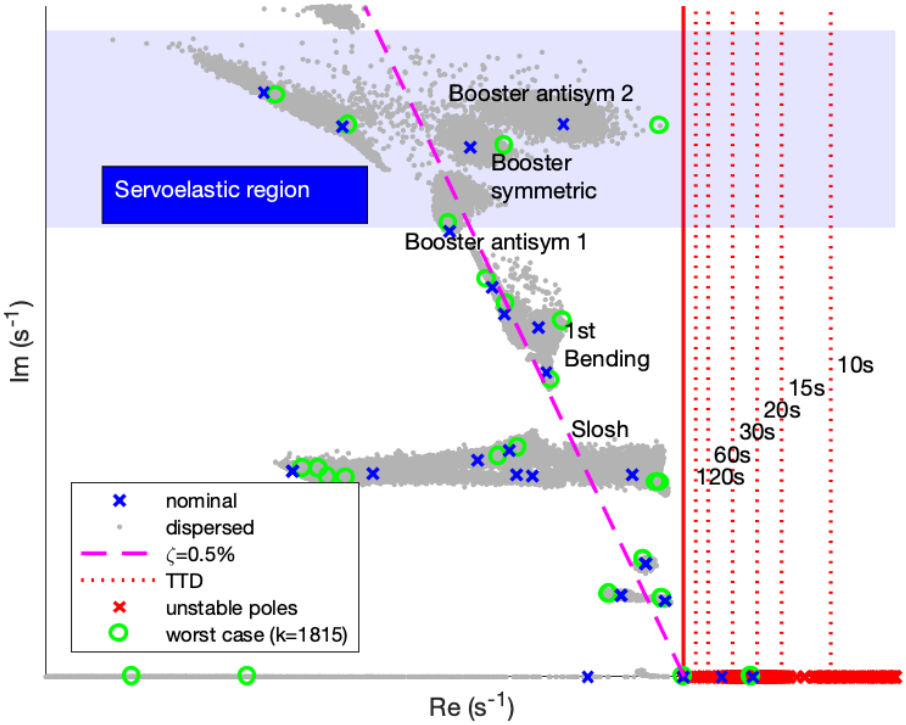

Figure 6. TVSE Effect on Open-Loop System Poles Without Autopilot Feedback

depends on the response of the actuator to load torques, the lighter (ablated) nozzle is less strongly coupled to the bending dynamics.

The RSRMV mode shape for this otherwise complex structure is nearly identical to the analytical solution of a free-free Euler-Bernoulli beam, thus allowing straightforward evaluation of the assumptions discussed in Section 3.2 for terms requiring higher-order spatial derivatives that are not generated by finite element modeling. Jet damping was shown to have a universally stabilizing effect for the first bending mode of long, solid rocket motors having uniform-beam-like mode shapes, reducing the sensitivity of SLS to TVSE.

The effect of TVSE and jet damping on the booster bending modes can be seen in Figure 6. For comparison, the constant line of $\zeta = 0.005$ (uncoupled) structural damping is shown along with the nominal and dispersed (Monte Carlo, $N = 2000$) system poles. At this flight condition with no jet damping, the bare structure with TVC servoloops closed exhibits a servoelastic instability at high frequency, exhibited by a complex pole pair with a relatively long time-to-double (TTD). However, inclusion of the case and nozzle rotation jet damping effects shifts the population of TVSE mode roots to a region that, under conservative assumptions, is more than adequate for vehicle loads and flight control stability.

Finally, the flight control system autopilot feedback, due to the fundamental motion of the core stage structure in torsion, provides a rate gyro signal that is always out of phase with the TVSE response. This has the convenient effect of phase stabilizing, or actively damping, the TVSE mode. Monte Carlo analysis under worst-on-worst parameter dispersions confirmed that the autopilot feedback will always add damping to even unstable TVSE dynamics. Further risk reduction was achieved by demonstrating in high-fidelity, nonlinear time domain simulation, implementing a

model similar to that discussed in Section 3.2, that a physically unrealistic but simulated inversion of autopilot feedback results in only a benign TVC limit cycle under worst-case conditions.

5 DISCUSSION

A comprehensive approach to the analysis and simulation of thrust vector servoelasticity and its application to the SLS vehicle has been presented. While such advanced formulations are not necessary for many booster configurations, designers should consider evaluating TVSE sensitivity for high-thrust, TVC-actuated systems early in the design phase, and assess whether a higher-fidelity analysis may be necessary. In the case of SLS, the TVSE phenomenon involved three-dimensional antisymmetric motion of the structure interacting with the very high thrust of the solid rocket boosters. Traditional planar models of the vehicle dynamics would not have uncovered the phenomenon.

A retrospective look at Space Shuttle flight dynamics models and data concludes that TVSE was not a concern, nor was it observed, in the Shuttle ascent configuration. The hydraulic TVC actuators used on the SLS boosters are the same as those used by the Shuttle SRMs. While this design has extensive flight heritage and is very reliable, its inner loop frequency response is essentially fixed by the hardware and allows limited flexibility to address actuator-level structural interactions. Counter to the expectation of the well-intentioned 1970s-era actuator designers, the performance characteristics of the booster TVC hardware (particularly the near total absence of internal mechanical nonlinearities) tend to exacerbate structural coupling behaviors.

Further analysis reveals that while the Shuttle ascent stack did exhibit a similar antisymmetric bending mode, the asymmetry in the structure strongly coupled this mode with wing bending, resulting in observed damping for small excitations in ground vibration testing on the order of 1.5%. At these damping levels, the coupling with the structure is of no consequence. More importantly, the higher-performance nozzle used on the SLS booster has a significantly higher moveable moment of inertia, which decreases the actuator bandwidth and increases the tendency for coupling.

The analysis, assessment, and resolution of TVSE on the SLS vehicle is another example of an unintended system-level consequence that can occur when employing seemingly low-risk heritage hardware to a new integrated vehicle configuration. The demands of performance and efficiency in launch vehicle designs inevitably result in a system that is much more sensitive to global interactions, where seemingly innocuous changes combine in such a way to challenge the design, or at least require a significant amount of analysis machinery to resolve.

REFERENCES

[1] Barrows, T., “Analysis of Engine/Flex Interaction Using a Second-Order SRB Actuator Model,” NASA MSFC internal memo, January, 2017.

[2] Donahue, B., "The Space Launch System: Development Progress," AIAA SPACE 2016, AIAA SPACE Forum, Long Beach, CA, September 2016, AIAA 2016-5415.

[3] Ballard, R., “SSME to RS-25: Challenges of Adapting a Heritage Engine to a New Vehicle Architecture,” Proc. Sixth European Conference for Aeronautics and Space Sciences (EUCASS), Krakow, Poland, June 2015.

[4] Orr, J., “A Flight Dynamics Model for a Multi-Actuated Flexible Rocket Vehicle,” AIAA Atmospheric Flight Mechanics Conference, Portland, OR, AIAA-2011-6563, August 2011.

[5] Frosch, J. and Vallely, D., “Saturn AS-501/S-IC Flight Control System Design,” J. Spacecraft, Vol. 4, No. 8, 1967, p. 1003-1009.

[6] Barrows, T. and Orr, J., “Jet Damping in FRACTAL,” NASA MSFC internal memo, November, 2017.

[7] Boyd, S., Convex Optimization, Cambridge University Press, 2004.